Dust Destruction by Charging: A Possible Origin of Gray Extinction Curves of Active Galactic Nuclei

Ryo Tazaki[1] , Kohei Ichikawa[1,2] , and Mitsuru Kokubo[1]
[1] Astronomical Institute, Graduate School of Science Tohoku University, 6–3 Aramaki, Aoba-ku, Sendai 980-8578, Japan; rtazaki@astr.tohoku.ac.jp
[2] Frontier Research Institute for Interdisciplinary Sciences, Tohoku University, Sendai 980-8578, Japan
Received 2020 January 22; revised 2020 February 18; accepted 2020 February 18; published 2020 March 31

Abstract

Observed extinction curves of active galactic nuclei (AGNs) are significantly different from those observed in the Milky Way. The observations require preferential removal of small grains at the AGN environment; however, the physics for this remains unclear. In this paper, we propose that dust destruction by charging, or Coulomb explosion, may be responsible for AGN extinction curves. Harsh AGN radiation makes a dust grain highly charged through photoelectric emission, and grain fission via Coulomb explosion occurs when the electrostatic tensile stress of a charge grain exceeds its tensile strength. We show that Coulomb explosion can preferentially remove both small silicate and graphite grains and successfully reproduce both flat extinction curve and the absence of 2175 Å bump.

Unified Astronomy Thesaurus concepts: Active galactic nuclei (16); Astrophysical dust processes (99); Ultraviolet extinction (1738)

1. Introduction

Dust is a crucial component of active galactic nuclei (AGNs; Urry & Padovani 1995). Recently, mid-infrared interferometric observations have revealed the presence of dust grains at polar regions at parsec scales (Hönig et al. 2012, 2013; Tristram et al. 2014; López-Gonzaga et al. 2016; Leftley et al. 2018; Hönig 2019). These polar dust grains are thought to be irradiated by harsh AGN radiation almost directly, and grain properties could be different from those observed in the local interstellar medium (e.g., Laor & Draine 1993).

The wavelength dependence of extinction at ultraviolet wavelengths is a powerful tool to infer dust properties at the polar region because grain properties are imprinted in the extinction curves (e.g., Li 2007). Previous observations have shown that AGN extinction curves are significantly different from those observed in the Milky Way (e.g., Maiolino et al. 2001a, 2001b, 2004; Gallerani et al. 2010; Hjorth et al. 2013). Major properties of AGN extinction curves are (i) flat wavelength dependence at far-ultraviolet wavelengths and (ii) the absence of a 2175 Å bump (Czerny et al. 2004; Gaskell et al. 2004; Gaskell & Benker 2007), which is thought to be caused by small graphite grains and/or polycyclic aromatic hydrocarbon (PAH) nanoparticles (e.g., Draine & Lee 1984; Weingartner & Draine 2001a; Compiègne et al. 2011). These observations imply that small grains, in particular for graphite grains, are preferentially removed from the AGN environments.

Several mechanisms have been proposed to explain the depletion of small grains, such as thermal sublimation and sputtering (Laor & Draine 1993); however, these models seem to fail. The sublimation is more likely to remove silicate grains rather than graphite grains, which is not consistent with observations (e.g., Gaskell et al. 2004). Chemisputtering might also preferentially destroy hot graphite grains (Barlow 1978; Draine 1979); however, it might be suppressed for a highly charged grain as thermal sputtering is suppressed in the vicinity of an AGN (e.g., Tazaki & Ichikawa 2020). In addition, drift-induced sputtering may not be an efficient mechanism for destroying small grains ($\lesssim 0.1\,\mu$m) because Coulomb coupling

between gas and the grains tends to halt hypersonic drift (Tazaki & Ichikawa 2020). Although Hoang et al. (2019) pointed out rotational disruption recently, this mechanism is also inefficient for disrupting small grains. If a 2175 Å bump is associated with PAH nanoparticles (e.g., Li & Draine 2001), these small grains might be disrupted by stochastic heating at around the AGN, although this possibility is also inconclusive. Hence, to date, a physical process responsible for flat and featureless extinction curves is still a matter of debate.

In this paper, we propose a new scenario for the origin of AGN extinction curves: dust destruction by charging, or Coulomb explosion (e.g., Draine & Salpeter 1979; Weingartner et al. 2006). Dust destruction by charging has been discussed in the field of gamma-ray bursts (Waxman & Draine 2000; Fruchter et al. 2001); however, such an effect has been overlooked in interpreting AGN extinction curves. Since Weingartner et al. (2006) have shown that a Coulomb explosion can occur even if grains are 100 pc away from quasar, it is naturally anticipated that such a process may significantly alter grain properties at a parsec-scale AGN environment.

In this paper, we study how dust destruction by charging affects AGN extinction curves and compare our model with a previously suggested thermal sublimation model. This paper is organized as follows. In Section 2, we summarize methods to calculate Coulomb explosion and thermal sublimation. Extinction curves predicted by dust destruction models are presented in Section 3. Sections 4 and 5 present a discussion and summary, respectively.

2. Methods and Models

2.1. AGN Environment

The radiation spectra of AGNs are taken from Nenkova et al. (2008), and the bolometric luminosity is assumed to be $L_{\mathrm{AGN}} = 10^{45}$ erg s^{-1}. For convenience, we define $L_{45} = (L_{\mathrm{AGN}}/10^{45}$ erg s$^{-1})$. Since we focus on grains at the polar region, where grains are thought to be irradiated by AGN radiation directly, we ignore the attenuation of AGN radiation.

At the parsec-scale polar region, radiation-hydrodynamic simulations suggest that the gas temperature and density are about $T_g \approx 10^4$ K and $n_H \approx 10 - 10^3$ cm^{-3}, respectively (Wada et al. 2016). Hence, we adopt $T_g = 10^4$ K and $n_H = 10^2$ cm^{-3} as a fiducial set of parameters. For the sake of simplicity, we assume T_g and n_H are constants.

2.2. Grain Charge

Dust grains become positively charged in the AGN environments (Weingartner et al. 2006). We compute grain charge Z_d (in the electron charge unit) by solving the rate equation (Weingartner et al. 2006; Tazaki & Ichikawa 2020):

$$\frac{dZ_d}{dt} = J_{pe} - J_e + J_{sec,gas} + J_{ion}, \qquad (1)$$

where J_{pe} is the photoelectric emission rate (Weingartner & Draine 2001b; Weingartner et al. 2006), J_e and J_{ion} are the collisional charging rate of electrons and ions, respectively (Draine & Sutin 1987), and $J_{sec,gas}$ is the rate for secondary electron emission induced by incident gas-phase electrons (Draine & Salpeter 1979). A typical charging timescale of a neutral grain due to electron collisions is $J_e^{-1} \sim 0.9$ s (Draine & Sutin 1987), where $T_g = 10^4$ K, the grain radius $a = 0.1 \, \mu$m, the electron density $n_e = 10^2$ cm^{-3}, and the sticking probability of 0.5 (Draine & Sutin 1987) are used. Since the charging timescale is much shorter than the dynamical timescale, we can assume the steady state in Equation (1). In addition, we can also ignore grain-charge distribution because the single-charge equilibrium approximation gives reliable results for highly charged grains (Weingartner et al. 2006). Thus, in this paper, we solve $J_{pe} - J_e + J_{sec,gas} + J_{ion} = 0$ to find Z_d.

It is useful to introduce the ionization parameter, $U_{ion} \equiv n_\gamma / n_H$, where n_γ is the total photon number density beyond 13.6 eV. Since the grain charge is mostly determined by the balance of photoelectric emission and electron collisions, U_{ion} characterizes the grain-charge amount. For the radiation spectra of AGNs used in Nenkova et al. (2008), we obtain

$$n_\gamma = 2.61 \times 10^6 \text{ cm}^{-3} \left(\frac{L_{AGN}}{10^{45} \text{ erg s}^{-1}} \right) \left(\frac{r}{\text{pc}} \right)^{-2}, \qquad (2)$$

where r is the distance from the central engine of the AGN. As a result, the ionization parameter becomes

$$U_{ion} = 2.61 \times 10^4 \left(\frac{n_H}{10^2 \text{ cm}^{-3}} \right)^{-1} \left(\frac{L_{AGN}}{10^{45} \text{ erg s}^{-1}} \right) \left(\frac{r}{\text{pc}} \right)^{-2}. \qquad (3)$$

2.3. Grain Temperature

The grain temperature, T_d, is obtained from the radiative equilibrium:

$$\frac{L_{AGN}}{4\pi r^2} \pi a^2 \langle Q_{abs} \rangle_{AGN} = 4\pi a^2 \sigma_{SB} T_d^4 \langle Q_{abs} \rangle_{T_d}, \qquad (4)$$

where r is the distance from the AGN, $\langle Q_{abs} \rangle_{AGN}$ and $\langle Q_{abs} \rangle_{T_d}$ are the AGN-spectrum averaged absorption efficiency and Planck mean absorption efficiency at dust temperature T_d, respectively, and σ_{SB} is the Stefan–Boltzmann constant. The

absorption efficiency, Q_{abs}, is calculated by using the Mie theory (Bohren & Huffman 1983), and the optical constant of silicate grains was taken from Draine & Lee (1984), Laor & Draine (1993), and Draine (2003). For graphite, the optical constant is calculated by adding the interband and free electron contributions (see also Draine & Lee 1984; Laor & Draine 1993; Draine 2003), where we adopt free electron models of Aniano et al. (2012). If the size parameter $x = 2\pi a / \lambda$, where λ is the wavelength, is larger than 2×10^4, we use the anomalous diffraction approximation (van de Hulst 1957) instead of using the Mie theory.

2.4. Grain Destruction Processes

We consider two kinds of dust destruction: Coulomb explosion (Section 2.4.1) and thermal sublimation (Section 2.4.2).
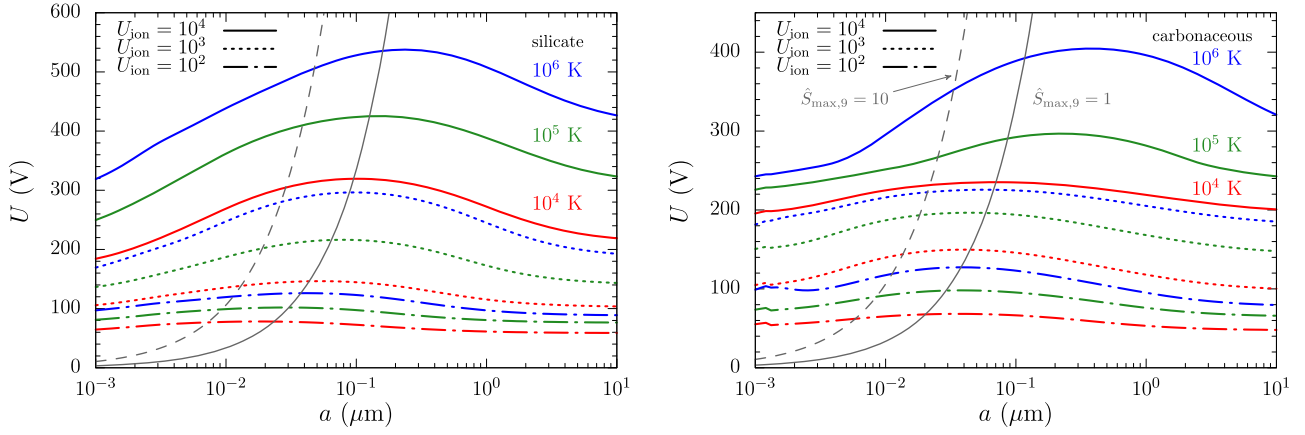
2.4.1. Coulomb Explosion

If a dust grain acquires a large amount of positive charges, Coulomb repulsion force within the grain causes grain fission, so-called Coulomb explosion (Draine & Salpeter 1979). The condition for Coulomb explosion is (Draine & Salpeter 1979)

$$S = \frac{1}{4\pi} \left(\frac{U}{a} \right)^2 \geqslant S_{max}, \qquad (5)$$

where S is the tensile stress in a charged sphere, $U = Z_d e / a$ is the electrostatic grain potential, and S_{max} is the tensile strength of the material. In the following, we use the normalized tensile strength defined by $\hat{S}_{max,9} = (S_{max}/10^9 \text{ erg cm}^{-3})$.

If the grain potential satisfies $U(a) \geqslant a(4\pi S_{max})^{1/2}$, the electric stress exceeds the tensile strength of a grain, and then Coulomb explosion will occur. We define the critical grain radius for Coulomb explosion, a_{CE}, such that $U(a_{CE}) = a_{CE}(4\pi S_{max})^{1/2}$. Grains smaller than a_{CE} are subjected to Coulomb explosion. Coulomb explosion will produce fragments of smaller grains. However, smaller fragments will be also charged enough to cause Coulomb explosion. Hence, we expect that a cascade fragmentation of grains due to Coulomb explosion occurs.

The tensile strength of a dust grain depends on material properties, such as composition and crystallinity. Although the tensile strength of cosmic dust particles is highly uncertain, laboratory measurements give us an estimate (see Hoang et al. 2019 for a summary of tensile strength). The tensile strength of graphite (polycrystalline) is suggested to be about $\hat{S}_{max,9} = 0.5 - 1$ (Burke & Silk 1974). Hence, in this study, we adopt the conservative value of $\hat{S}_{max,9} = 1$ for graphite grains. The tensile strength of forsterite (silicate) can be as small as $\hat{S}_{max,9} = 1.21$ (Gouriet et al. 2019). Meanwhile, MacMillan (1972) reported the tensile strength of glass rods and fibers is about $\hat{S}_{max,9} = 130$. We adopt the values of $\hat{S}_{max,9} = 10$ for silicate. It is worth noting that the above measurements are based on bulk materials, and therefore small grains may have different values of tensile strength. Since the tensile strength is an uncertain parameter, we discuss how S_{max} changes our results in Section 3.

Figure 1. Electrostatic potential, $U = eZ_d/a$, for silicate grains (left) and carbonaceous grains (right). Solid, dotted, and dotted–dashed lines represent the results for $U_{ion} = 10^4$, 10^3, and 10^2, respectively. Blue, green, and red colors represent gas temperature $T_g = 10^6$ K, 10^5 K, and 10^4 K, respectively. Gray solid and dashed lines represent the threshold for Coulomb explosion for grains of the tensile strength $\hat{S}_{max,9} = 1$ and 10, respectively.

2.4.2. Thermal Sublimation

The sublimation temperature of dust grains, T_{sub}, is determined by a balance between gas pressure and saturation pressure (Guhathakurta & Draine 1989; Baskin & Laor 2018). By using Equation (27) in Baskin & Laor (2018), we compute T_{sub} with the the standard solar elemental abundances (Grevesse & Sauval 1998). As a result, we obtain $T_{sub} = 1322$ K for graphite and $T_{sub} = 1072$ K for silicate grains when $n_H = 10^2$ cm^{-3} and $T_g = 10^4$ K.

Since smaller grains are usually hotter than larger grains, they can preferentially sublimate (e.g., Laor & Draine 1993). We can define critical grain radius for thermal sublimation such that $T_d(a_{sub}) = T_{sub}$. Grains smaller than a_{sub} will sublimate.

3. Results

3.1. Electrostatic Grain Potential

We first solve Equation (1) with the steady-state assumption, and the results are presented in Figure 1. As a general tendency, higher U_{ion} and T_g give larger grain electrostatic potential. Our calculations quantitatively agree with Weingartner et al. (2006), although assumed radiation spectra are not the same.

Figure 1 shows that the grain potential depends on the grain radius and becomes maximum at the submicron sizes, while grain charge Z_d is a monotonically increasing function of grain radius. This is mainly determined by two competing effects: photoelectric yield and photon absorption efficiency. With decreasing grain radius, the photoelectric yield is increased due to the small particle effect (e.g., Watson 1973; Draine 1978). Hence, smaller grains are more likely to emit photoelectrons once a high-energy photon is absorbed. However, decreasing grain radius reduces the absorption efficiency of photons, once the grain radius is smaller than the incident radiation wavelength, which is typically about $\lambda \sim 0.1$ μm. Hence, due to lower photon absorption efficiency, the photoelectric emission rate is decreased, and therefore the grain potential is decreased for smaller grains ($a \lesssim 0.1$ μm). Because of these two effects, the grain potential is maximized at submicron sizes. Although the grain potential also depends on the grain composition, silicate and graphite grains have almost similar grain potential.

Figure 1 also shows that the critical grain size for Coulomb explosion is about $a_{CE} \sim 0.01 - 0.1$ μm for $U_{ion} = 10^2 - 10^4$ and $T_g = 10^4 - 10^6$ K at $\hat{S}_{max,9} = 1$.

3.2. Coulomb Explosion versus Thermal Sublimation
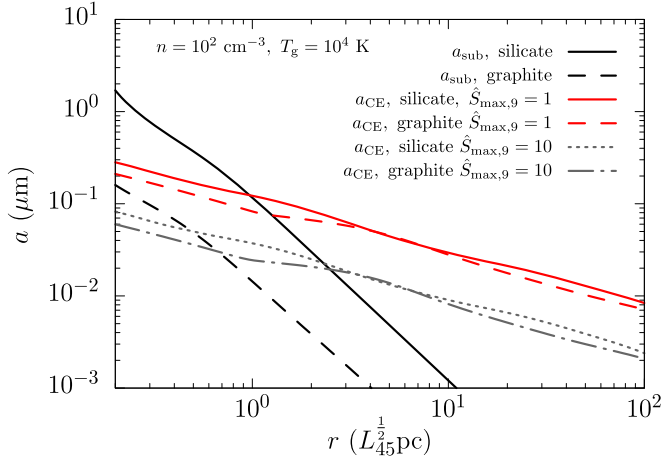
Next, we compare a_{CE} and a_{sub} as well as their radial dependence from the center of the AGN. Figure 2 shows the critical grain radii a_{sub} and a_{CE} for both silicate and graphite composition as a function of the distance from the AGN. It is found that a_{CE} has shallower radial dependence than a_{sub}. The radial dependence of the critical grain radius for sublimation is about $a_{sub} \propto r^{-2}$. As long as the Rayleigh approximation is valid, that is, the wavelength of thermal emission is longer than the grain radius, we have $\langle Q_{abs}\rangle_{T_d} \propto a$. Hence, for a fixed dust temperature ($T_d = T_{sub}$), Equation (4) results in $a_{sub} \propto r^{-2}$. In other words, a_{sub} is proportional to the radiative flux from the AGN.

Grain charging seems to be caused also by the radiation flux, since a grain is charged via photoelectric emission. However, grain potential is *not* proportional to r^{-2}. For example, in Figure 1, even if U_{ion} ($\propto$ radiative flux) decreases by an order of magnitude, grain potential U decreases only by a factor of few. These results suggest that Coulomb explosion can be important at larger distances, e.g., parsec-scale distance.

Figure 2 also shows that a difference in a_{CE} between graphite and silicate grains is not so large compared to the difference seen in a_{sub}. Thus, Coulomb explosion tends to remove both silicate and graphite grains of almost similar grain radii. Meanwhile, for sublimation, the graphite grains have smaller a_{sub} because (1) the emissivity at near-infrared wavelength is higher, and (2) T_{sub} is higher (see also Laor & Draine 1993; Baskin & Laor 2018). Therefore, this suggests that thermal sublimation preferentially removes small silicate grains rather than graphite grains.

3.3. Extinction Curves

To understand how thermal sublimation or Coulomb explosion change extinction curves, we compute an extinction cross section of grains. We assume that the grain size distribution obeys $dn_i \propto \mathcal{A}_i a^{-3.5} da$ ($a_{min}^i \leqslant a \leqslant a_{max}$), where dn_i is the number density of dust grains of type i (silicate or graphite) in a size range $[a, a + da]$, and $\mathcal{A}_i$ is the abundance

Figure 2. Grain radius against a distance from the AGN. Black and red lines indicate a_{sub} and a_{CE}, respectively, where a_{CE} is computed for $\hat{S}_{max,9} = 1$ for both silicate and graphite grains. Solid and dashed lines indicate silicate and graphite grains, respectively. Gray dotted and dashed–dotted lines are a_{CE} for $\hat{S}_{max,9} = 10$ for both graphite and silicate grains, respectively. Grains with $a \lesssim a_{sub}$, a_{CE} will be disrupted.

of the grain type i (Draine & Lee 1984). We set $a_{min}^{i} = \max(a_{sub}^{i}, \quad a_{CE}^{i}, \quad a_{min,MRN})$, where $a_{min,MRN} = 0.005 \, \mu$m. We treat a_{max} as a free parameter. We also set the abundance of silicate and graphite from Draine & Lee (1984). The extinction magnitude at wavelength λ, A_λ, is
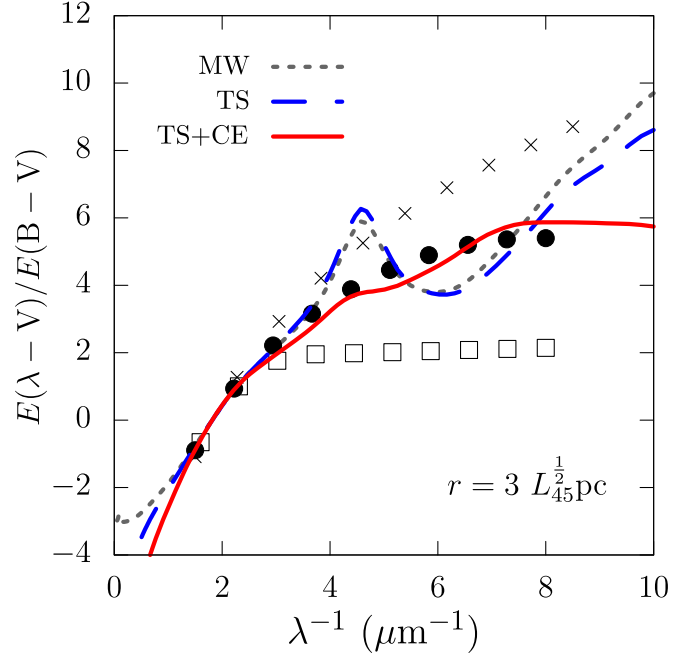
$$A_\lambda \propto \sum_i \int C_{ext}^{i}(\lambda, a) \frac{dn_i}{da} da, \qquad (6)$$

where $C_{ext}^{i}(\lambda, a)$ is the extinction cross section of a grain of type i with radius a. We define the extinction curve as $E(\lambda - V)/E(B - V) = (A_\lambda - A_V)/(A_B - A_V)$, where A_V and A_B are the extinctions at visual (5500 Å) and blue (4400 Å) wavelengths.

Figure 3 shows the extinction curves with/without Coulomb explosion at $3L_{45}^{\frac{1}{2}}$ pc away from the nucleus. The extinction curve with Coulomb explosion can successfully reproduce a flat extinction curve as well as the absence of a 2175 Å bump. In addition, the predicted extinction curve is consistent with the observation by Gaskell & Benker (2007). Meanwhile, the extinction curve without Coulomb explosion, or $a_{min}^{i} = \max(a_{sub}^{i}, a_{min,MRN})$, shows a prominent 2175 Å bump. This is because sublimation does not remove small graphite grains, although small silicate grains are removed (Figure 2). Since observed AGN extinction curves do not show such a bump (Czerny et al. 2004; Gaskell et al. 2004; Gaskell & Benker 2007), the sublimation model is insufficient to reproduce observed extinction curves.

Figure 4 shows extinction curves at various radial distances. Even if the radial distances are changed, the overall shape of the extinction curve with Coulomb explosion is still similar to the one from Gaskell & Benker (2007) up to $r \simeq 10L_{45}^{\frac{1}{2}}$ pc, while the thermal sublimation model remains inconsistent with observations. When increasing the distance from the AGN, U_{ion} decreases, and then smaller grains can survive from Coulomb explosion; nevertheless, 2175 Å is still weak for the model with Coulomb explosion.

Extinction curves with Coulomb explosion are not sensitive to the choice of maximum grain radius as long as it is larger than 0.25 μm (Figure 5). When grain radius is smaller this

Figure 3. Extinction curves with and without Coulomb explosion are shown in red solid and blue dashed lines, respectively. For reference, the gray short-dashed line is the average Milky Way extinction curve, which is computed with $a_{min} = 0.005 \, \mu$m and $a_{max} = 0.25 \mu$m. Circles indicate observed values taken from Gaskell & Benker (2007), whereas crosses and squares indicate those taken from Czerny et al. (2004) and Gaskell et al. (2004), respectively. We assume $a_{max} = 1 \, \mu$m.

value, the extinction curve steeply increases with decreasing wavelength.
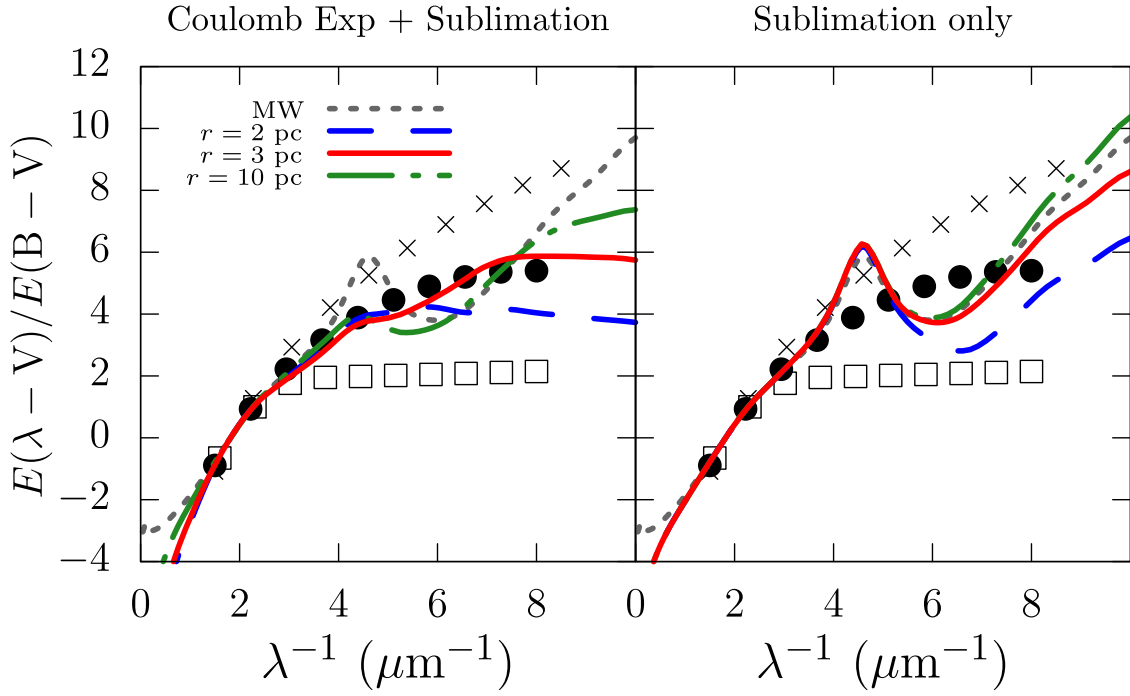
Extinction curves with Coulomb explosion are found to be similar to those observed by Gaskell & Benker (2007). In addition, if the maximum grain radius is smaller than 0.25 μm, the curves become similar to those observed by Czerny et al. (2004). However, our model fails to explain observations by Gaskell et al. (2004). Explaining such extinction curves might require an additional mechanism, such as a reduced-graphite abundance (Gaskell et al. 2004).
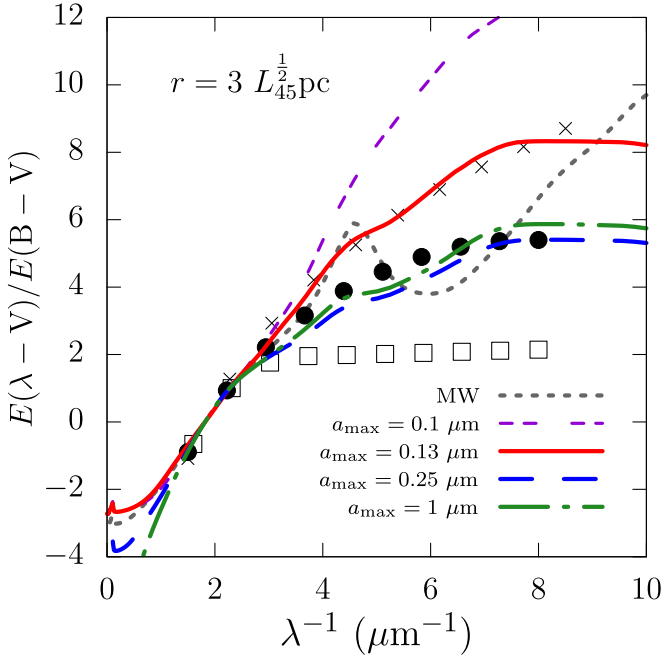
4. Discussion

4.1. Comparison with Observations of the Torus Innermost Radius

We have shown that the Coulomb explosion can be a more important process for dust destruction than thermal sublimation. Meanwhile, near-IR dust reverberation mapping observations for AGNs, which show that the color temperatures of the variable hot dust emission agree with the dust sublimation temperature (1400 − 2000 K), and the innermost radius of the dust torus R_{in} is proportional to the square root of the AGN luminosity ($R_{in} \propto L_{AGN}^{1/2}$), strongly suggest that the dust innermost radius is determined by the thermal sublimation (Koshida et al. 2014; Yoshii et al. 2014; Minezaki et al. 2019; Gravity Collaboration et al. 2020 and references therein). This apparent conflict can be attributable to the difference of gas density.

While the ambient gas density of $n_H = 10^2 \, cm^{-3}$ assumed throughout the calculations in this work is a reasonable assumption for the outflowing gas at the polar region of AGNs, the gas density of the equatorial dust torus is expected to be much higher. The gas at the innermost part of the dust torus can be as dense as broad emission line regions, where
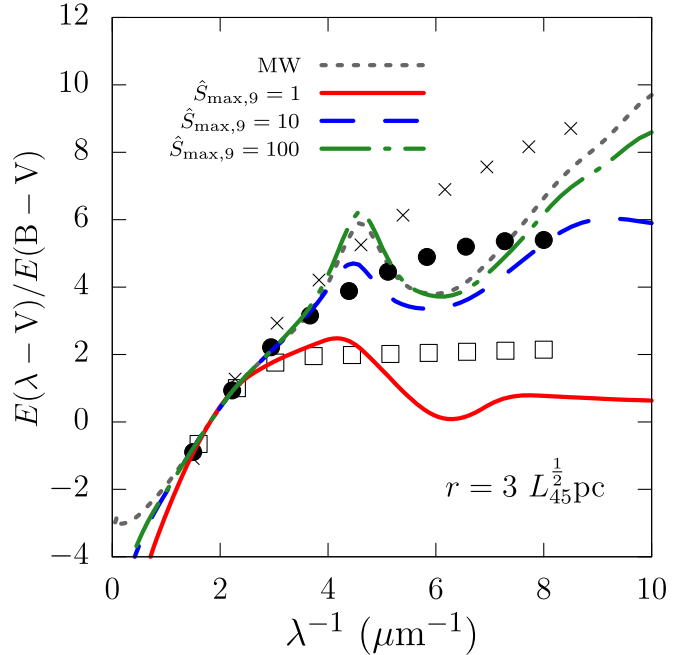
Coulomb Exp + Sublimation

Sublimation only

Figure 4. Same as Figure 3, but for different distances from the AGN. For all lines, the AGN luminosity is set as $L_{45} = 1$. Left and right panels show the results with and without Coulomb explosion, respectively.

Figure 5. Extinction curves for various a_{max}, where tensile strength of graphite and silicate grains are $\hat{S}_{max,9} = 1$ and 10, respectively. $r = 3L_{45}^{\frac{1}{2}}$ pc is assumed. The gray short-dashed line shows the Milky Way values.

Figure 6. Predicted extinction curves by the Coulomb explosion model with various tensile strength values. Solid, dashed, and dotted–dashed lines correspond to $\hat{S}_{max,9} = 1$, 10, 100, respectively. Both silicate and graphite grains have the same tensile strength with an assumption of $a_{max} = 1 \mu m$.

$n_H \sim 10^{10}$ cm^{-3} (e.g., Baskin & Laor 2018; Kokubo & Minezaki 2020); in such a dense gas region, higher dust sublimation temperatures are expected ($T_{sub} = 1880$ K and 1503 K for graphite and silicate grains, respectively), and the importance of the Coulomb explosion relative to the thermal sublimation is significantly reduced due to inefficient grain charging by the enhanced electron collision rate (see Section 2.2). Therefore, unlike in the case of the polar dust region, the dust destruction at the innermost region of the

equatorial dust torus must be governed by the thermal sublimation.

4.2. Tensile Strength of Small Grains?

Coulomb explosion depends on the tensile strength assumed. Figure 6 shows how the tensile strength affects extinction curves. In Figure 6, both silicate and graphite grains are assumed to have the same tensile strength. As the tensile

strength increases, Coulomb explosion becomes inefficient, and then both small silicate and graphite grains can survive. As a result, extinction curves show an increase toward shorter wavelengths with a prominent 2175 Å bump. Hence, observed extinction curves, e.g., a lack of a 2175 Å bump, seems to be reproduced when $\hat{S}_{\mathrm{max},9} \lesssim 10$, and this is within a range of measured values for bulk materials (e.g., Section 2.4.1).

Under the assumption of the tensile strength for bulk materials determined by laboratory experiments, the Coulomb explosion leads to the absence of small dust grains in close vicinity to AGNs and thus can naturally explain the observed flat extinction curve. Conversely, if the tensile strength of the cosmic dust is far stronger than that for the bulk materials due to, e.g., crystallization by annealing for hot small grains, the graphite grains survive even under the large electrostatic potential and a 2175 Å bump feature is unavoidable. Therefore, if our scenario for the flat extinction curve by the Coulomb explosion is true, it also suggests that the tensile strength of the cosmic dust must be close to the value of the bulk materials. However, we should keep in mind that if PAH nanoparticles are the carrier of a 2175 Å bump, the bump might be suppressed by destroying these particles as suggested by observations (e.g., Sturm et al. 2000).

5. Conclusion

In this paper, we have shown that thermal sublimation is insufficient to reproduce observed AGN extinction curves because this model predicts too strong of a 2175 Å bump due to preferential survival of small graphite grains. We have proposed that Coulomb explosion can successfully reproduces flat extinction curves as well as the absence of 2175 Å bump as long as the tensile strength is lower than 10^{10} erg cm^{-3}. The predicted extinction curves have shown to be very similar to those observed by Gaskell & Benker (2007) as well as Czerny et al. (2004). The Coulomb explosion model implies that the variety of radiation environment (U_{ion}) and maximum grain radius may partly explain various types of observed AGN extinction curves (Czerny et al. 2004; Gaskell & Benker 2007).

ORCID iDs

Ryo Tazaki ● https://orcid.org/0000-0003-1451-6836
Kohei Ichikawa ● https://orcid.org/0000-0002-4377-903X
Mitsuru Kokubo ● https://orcid.org/0000-0001-6402-1415

References

Aniano, G., Draine, B. T., Calzetti, D., et al. 2012, ApJ, 756, 138
Barlow, M. J. 1978, MNRAS, 183, 397
Baskin, A., & Laor, A. 2018, MNRAS, 474, 1970
Bohren, C. F., & Huffman, D. R. 1983, Absorption and Scattering of Light by Small Particles (New York: Wiley)
Burke, J. R., & Silk, J. 1974, ApJ, 190, 1
Compiègne, M., Verstraete, L., Jones, A., et al. 2011, A&A, 525, A103
Czerny, B., Li, J., Loska, Z., & Szczerba, R. 2004, MNRAS, 348, L54
Draine, B. T. 1978, ApJS, 36, 595
Draine, B. T. 1979, ApJ, 230, 106
Draine, B. T. 2003, ApJ, 598, 1026
Draine, B. T., & Lee, H. M. 1984, ApJ, 285, 89
Draine, B. T., & Salpeter, E. E. 1979, ApJ, 231, 77
Draine, B. T., & Sutin, B. 1987, ApJ, 320, 803
Fruchter, A., Krolik, J. H., & Rhoads, J. E. 2001, ApJ, 563, 597
Gallerani, S., Maiolino, R., Juarez, Y., et al. 2010, A&A, 523, A85
Gaskell, C. M., & Benker, A. J. 2007, arXiv:0711.1013
Gaskell, C. M., Goosmann, R. W., Antonucci, R. R. J., & Whysong, D. H. 2004, ApJ, 616, 147
Gouriet, K., Carrez, P., & Cordier, P. 2019, Minerals, 9, 787
Gravity Collaboration, Pfuhl, O., Davies, R., et al. 2020, A&A, 634, A1
Grevesse, N., & Sauval, A. J. 1998, SSRv, 85, 161
Guhathakurta, P., & Draine, B. T. 1989, ApJ, 345, 230
Hjorth, J., Vreeswijk, P. M., Gall, C., & Watson, D. 2013, ApJ, 768, 173
Hoang, T., Tram, L. N., Lee, H., & Ahn, S.-H. 2019, NatAs, 3, 766
Hönig, S. F. 2019, ApJ, 884, 171
Hönig, S. F., Kishimoto, M., Antonucci, R., et al. 2012, ApJ, 755, 149
Hönig, S. F., Kishimoto, M., Tristram, K. R. W., et al. 2013, ApJ, 771, 87
Kokubo, M., & Minezaki, T. 2020, MNRAS, 491, 4615
Koshida, S., Minezaki, T., Yoshii, Y., et al. 2014, ApJ, 788, 159
Laor, A., & Draine, B. T. 1993, ApJ, 402, 441
Leftley, J. H., Tristram, K. R. W., Hönig, S. F., et al. 2018, ApJ, 862, 17
Li, A. 2007, in ASP Conf. Ser. 373, Dust in Active Galactic Nuclei, ed. L. C. Ho & J. W. Wang (San Francisco, CA: ASP), 561
Li, A., & Draine, B. T. 2001, ApJ, 554, 778
López-Gonzaga, N., Burtscher, L., Tristram, K. R. W., Meisenheimer, K., & Schartmann, M. 2016, A&A, 591, A47
MacMillan, N. H. 1972, JMatS, 7, 239
Maiolino, R., Marconi, A., & Oliva, E. 2001a, A&A, 365, 37
Maiolino, R., Marconi, A., Salvati, M., et al. 2001b, A&A, 365, 28
Maiolino, R., Schneider, R., Oliva, E., et al. 2004, Natur, 431, 533
Minezaki, T., Yoshii, Y., Kobayashi, Y., et al. 2019, ApJ, 886, 150
Nenkova, M., Sirocky, M. M., Ivezić, Ž., & Elitzur, M. 2008, ApJ, 685, 147
Sturm, E., Lutz, D., Tran, D., et al. 2000, A&A, 358, 481
Tazaki, R., & Ichikawa, K. 2020, ApJ, in press (doi:10.3847/1538-4357/ab72f6)
Tristram, K. R. W., Burtscher, L., Jaffe, W., et al. 2014, A&A, 563, A82
Urry, C. M., & Padovani, P. 1995, PASP, 107, 803
van de Hulst, H. C. 1957, Light Scattering by Small Particles (New York: Wiley)
Wada, K., Schartmann, M., & Meijerink, R. 2016, ApJL, 828, L19
Watson, W. D. 1973, JOSA, 63, 164
Waxman, E., & Draine, B. T. 2000, ApJ, 537, 796
Weingartner, J. C., & Draine, B. T. 2001a, ApJ, 548, 296
Weingartner, J. C., & Draine, B. T. 2001b, ApJS, 134, 263
Weingartner, J. C., Draine, B. T., & Barr, D. K. 2006, ApJ, 645, 1188
Yoshii, Y., Kobayashi, Y., Minezaki, T., Koshida, S., & Peterson, B. A. 2014, ApJL, 784, L11